Science Advances
AAAS

advances.sciencemag.org/cgi/content/full/4/8/eaat4978/DC1

Supplementary Materials for

Springtail-inspired superomniphobic surface with extreme pressure resistance

Geun-Tae Yun, Woo-Bin Jung, Myung Seok Oh, Gyu Min Jang, Jieung Baek, Nam Il Kim, Sung Gap Im, Hee-Tae Jung*

*Corresponding author. Email: heetae@kaist.ac.kr

Published 24 August 2018, *Sci. Adv.* **4**, eaat4978 (2018)
DOI: 10.1126/sciadv.aat4978

The PDF file includes:

Other Supplementary Material for this manuscript includes the following:

(available at advances.sciencemag.org/cgi/content/full/4/8/eaat4978/DC1)

Supplementary Text

1. Processes to fabricate hierarchical superomniphobic surface

The whole fabrication processes of the structured surfaces designed in this paper are shown. The control surfaces (hierarchical structure with disk- and overhang-shaped nanostructures) were fabricated with less steps than processes for the main surface with serif-T-shaped nanostructures. After surface structuring, an additional step of low surface energy polymer coating was required.

Hierarchical surface with disk-shaped nanostructures (fig. S4): Starting with gold dot nanopatterns formation (fig. S1), wrinkled surface was induced entirely by thermal shrinkage of PS substrate. Using polyvinylpyrolidone (PVP) as upper and protecting layer during processes, the structured surface was coated by 5 wt % of PVP solution with ethanol by spin coating. Followed by heat-induced shrinkage in oven at 135°C introduced microscale wrinkled structures over whole area. Afterwards wrinkled structures formation, the PVP layer was rinsed-off by ethanol. A ~ 40 nm-thick of poly-(3,3,4,4,5,5,6,6,7,7,8,8,9,9,10,10,10-heptadecafluorodecyl methacrylate (PHFDMA) was coated by iCVD method to tune the surface as low surface energy chemistry.

Hierarchical surface with overhang-shaped nanostructures (fig. S4): Starting with gold dot nanopatterns formation (fig. S1), the pillars underneath were fabricated by oxygen reactive ion etching (RIE). Using polymer-selective etching property of oxygen plasma, ~ 600 nm-height of PS pillars were etched isotropically over whole area. Followed wrinkling processes were performed to fabricate hierarchical system as described above. Afterwards wrinkled structures formation, the PVP layer was rinsed-off by ethanol. A ~ 40 nm-thick of PHFDMA was coated by iCVD method to tune the surface as low surface energy chemistry.

Hierarchical surface with serif-T-shaped nanostructures (Fig. 1): Starting with gold dot nanopatterns formation (fig. S1), the steps for sidewall structures were introduced to fabricate nanostructures with doubly reentrant feature. A PS substrate was etched anisotropically (~ 90 nm) by high vacuum RIE using gold dot nanopatterns as an etching mask. To proceed secondary sputtering lithography (SSL), an additional layer of gold (~ 20 nm) was deposited over structured surface. Followed by Ar^+ ion bombardment process etched additionally deposited gold layer and created a 15 nm-thick thin gold layer on pre-etched vertical PS wall. Afterwards head part with doubly reentrant feature fabrication, ~ 600 nm-height of PS pillars were etched isotropically over whole area by oxygen RIE. The surface studded with fabricated serif-T-shaped nanostructures was experienced the wrinkling processes described above for hierarchical system. A ~ 40 nm-thick of PHFDMA was coated by iCVD method to tune the surface as low surface energy chemistry.

2. Wetting characteristics provided by hierarchical system with serif-T-shaped nanostructures

By parameter analysis, the static repellency and high robustness to hydrodynamic pressure can be elucidated. The static repellency of surface is highly affected by solid-liquid contact fraction that is highly related with feature dimensions of structures. In addition, this can be parameterized as design parameter, D^*. D^* is the inverse of solid-liquid contact fraction Φ_s. From the Cassie-

Baxter equation, the relationship between D^* and apparent contact angle θ^* on the composite interfaces such as hierarchical system can be written as (*32*)

$$\cos\theta^* = -1 + \frac{1}{D^*}(1 + r_\Phi \cos\theta) \quad \text{(S1)}$$

where r_Φ is roughness of the structure and θ is the equilibrium Young's contact angle. Depending on wetting regime theory, as smaller the solid-liquids contact fraction and bigger the roughness of the surface, it is more beneficial to have Cassie-Baxter regime with higher apparent contact angle, which implies higher D^* is required for higher repellency. For getting – phobic characteristics ($\theta^* > 90°$) with certain liquids, D^* should be bigger than 1. In addition, the overall D^* value of hierarchical system with additional levels of texture can be determined by multiplying the D^* values of each individual scale of texture. Theoretically, the design parameter of fabricated nanostructures in this work, D^*_{nano}, can be calculated based on equation S2 (*8*)

$$D^* = \left(\frac{(W+D)}{W}\right)^2 \quad \text{(S2)}$$

where *W* is a diameter of head of nanostructures and *D* is a half of a spacing between adjacent nanostructures. Hence, in our design, D^*_{nano} is ~ 4 because both *W* and *D* are about 200 nm scale. In our design, microscale wrinkled surface can reduce solid-liquid contact fraction effectively by providing additional air pockets, which means design parameter $D^*_{\text{micro}} > 1$. As higher areal strain applied, the bigger D^*_{micro} could be achieved and leads to enhanced static repellency. As a result, design parameter of hierarchical system $D^*_{\text{hierarchical}} = D^*_{\text{nano}} \times D^*_{\text{micro}}$, which is more beneficial than single-scale texture. (Fig. 3)

In terms of robustness to hydrodynamic pressure, robustness parameter A^* is highly important, which is defined as (*8*)

$$\frac{1}{A^*} = \frac{1}{H^*} + \frac{1}{T^*}, where\ H^* = \frac{(1-cos\theta)Rl_{cap}}{D^2}, T^* = \frac{l_{cap}\sin(\theta-\psi_{min})}{2D} \quad \text{(S3)}$$

where l_{cap} is capillary length of liquid, R is curvature of head structure, and ψ_{min} is minimum texture angle for given surface. To get highly robust surface structure, A^* should be bigger than 1 and is more beneficial with bigger value. By structural control, the *D* and ψ_{min} can affect to robustness of surfaces. The serif-T-shaped nanostructures have *D* value that is smaller over three orders magnitude than microstructures, which have been proposed from almost previous reports, and ψ_{min} ~ - 90°, which is the ideal doubly reentrant feature for high robustness. These structural designs lead to around three order bigger magnitude for A^* value of serif-T-shaped nanostructures than doubly reentrant microstructures (*5*). As a result, artificial springtail surface studded with serif-T-shaped nanostructures showed extreme robustness. For microscale wrinkled structures, it does not provide significant enhancement for A^*, however, wetting reversibility in hierarchical textures can support how artificial springtail surface can show extreme resistance (*33*). As higher areal strain applied, the valley-like structures in fig. S5 increased break-through pressure of hierarchical system by yielding harder to penetrate. (Fig. 4, 5) The parameter analysis confirms the advantages of hierarchical system to overcome general trade-off between static repellency and robustness to pressure.

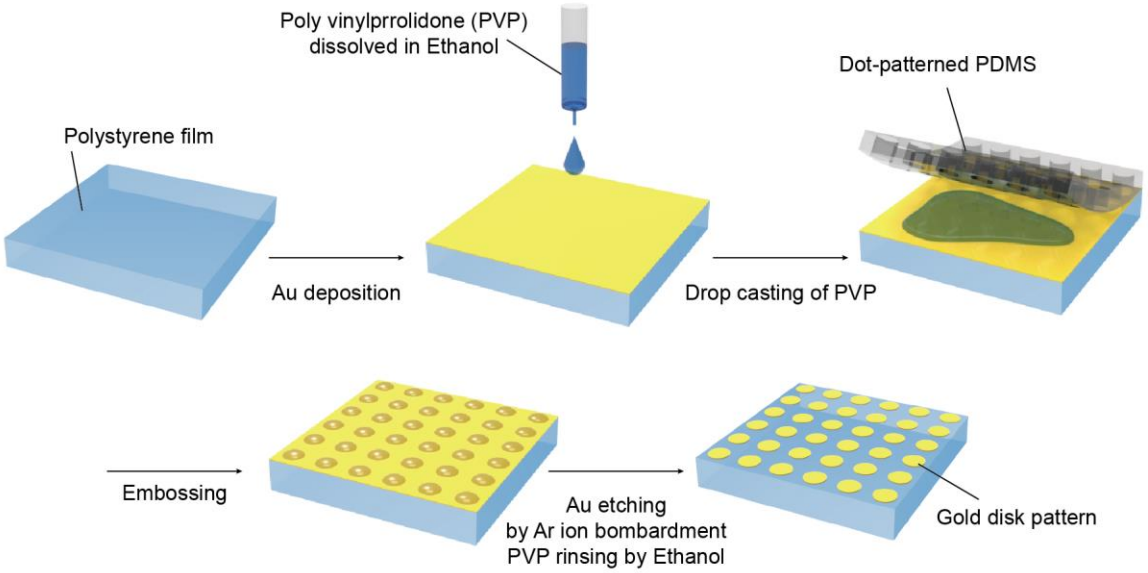

Fig. S1. Schematic illustration of gold dot nanopattern fabrication on PS substrate by using conventional nanoimprinting. Dot-patterned polyvinylpyrolidone (PVP) acts as an etching mask of deposited gold layer. Exposed gold was etched by Ar^+ ion bombardment.

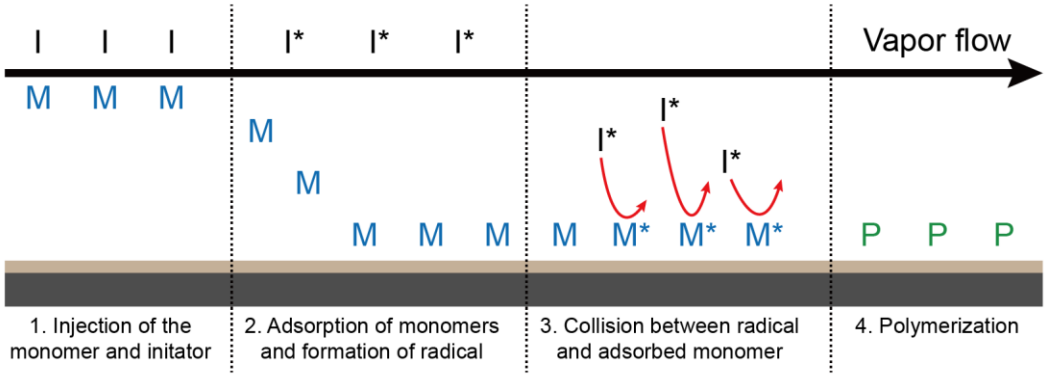

Fig. S2. Schematic illustration of polymer with low surface energy (PHFDMA) coating on structured surface by iCVD. Injected monomers and initiators of vapor phase formed uniform polymerized layer by 200 ~ 300℃ heated filament.

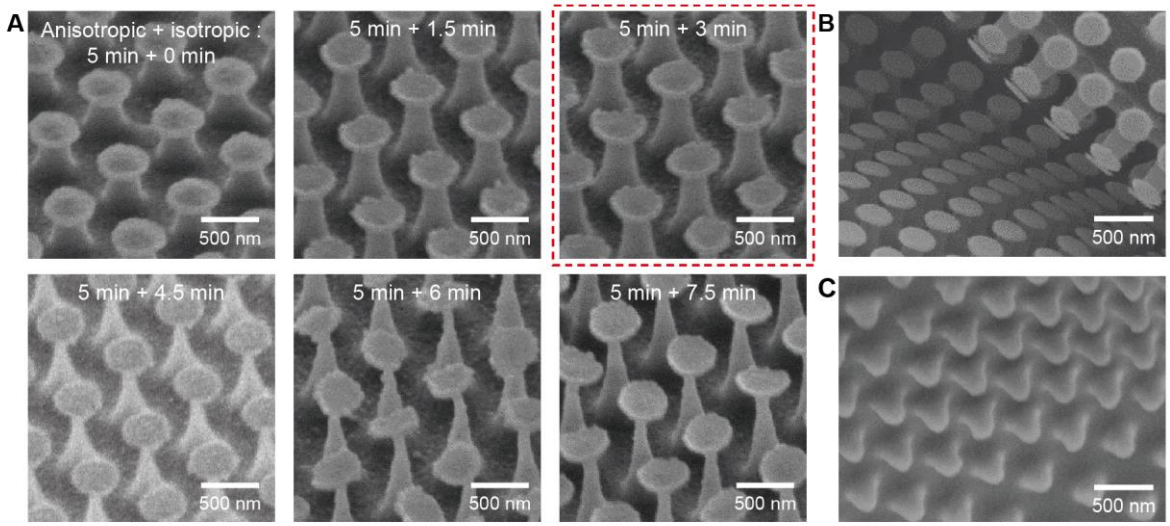

Fig. S3. SEM images of nanostructures with different pillar etching condition. (A) Pillars are etched with two steps by oxygen reactive ion etching (RIE), first step is set in low vacuum condition (~ 10^{-2} torr) with 5 minutes for isotropic etching and followed second step is set in high vacuum condition (~10^{-6} torr) with different time for anisotropic etching. **(B)** Well-fabricated nanostructures with first step for 5minutes and second step for 3 minutes. **(C)** Broken pillars after wrinkling process because of thinner pillar as more etching.

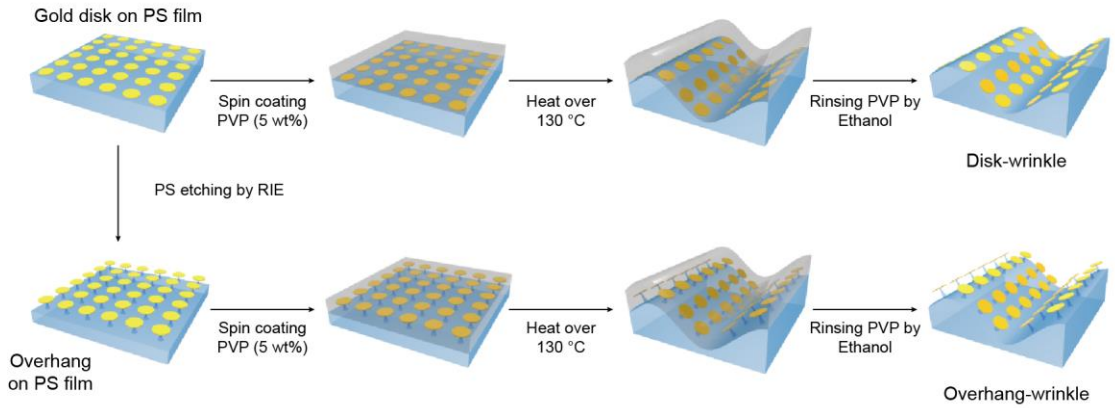

Fig. S4. Schematic illustration of fabrication for hierarchical system with overhang (reentrant)– and disk-shaped nanostructures. For disk-shaped system, just wrinkling process by heating is needed after dot patterns fabrication in fig. S1. However, for overhang-shaped system, additional etching for underneath pillars is needed.

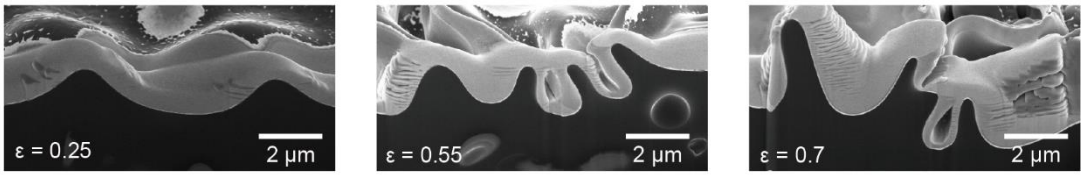

Fig. S5. Different morphologies of wrinkled surface with applied areal strain during wrinkling. For highly-wrinkled surface (ε = 0.7), the valley-like structures with high amplitude were observed.

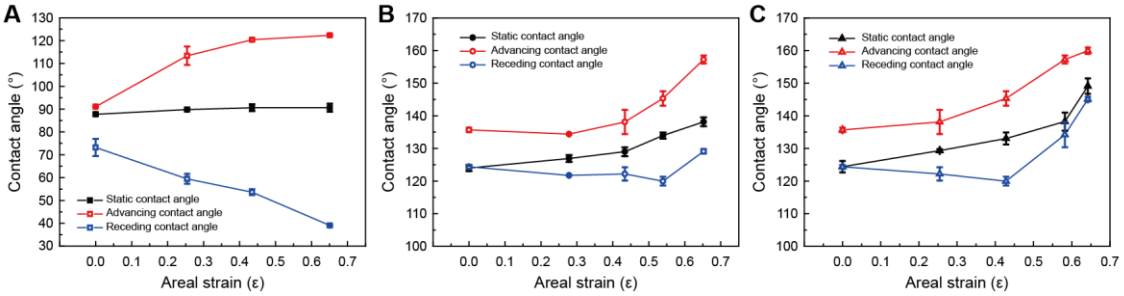

Fig. S6. Advancing and receding contact angles of ethanol on the three different nanostructures. Static, advancing and receding contact angles of ethanol on **(A)** disk, **(B)** overhang and **(C)** serif-T nanostructures with varying areal strain.

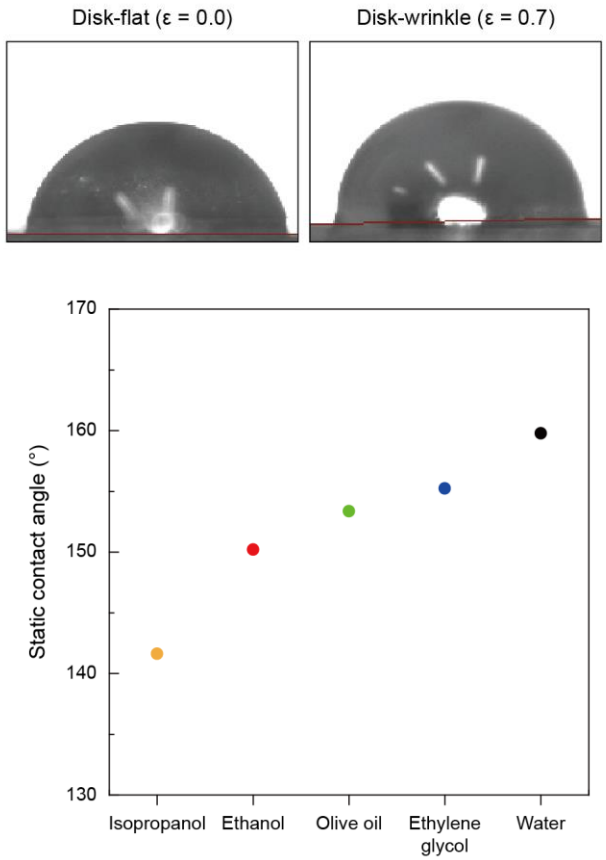

Fig. S7. Contact regimes of ethanol droplet on surface with disk-shaped nanostructures and contact angles of various liquids. Both on flat surface (ε = 0) with disk-shaped and on highly-wrinkled surface (ε = 0.7) with disk-shaped cannot show omniphobicity regardless of microscale wrinkle structures. As the lowest surface tension liquid, isopropanol (20.9 mN/m) shows 141.63 ° in static contact angle. Additionally, bean oil (31.2 mN/m) and olive oil (32.0 mN/m) show 152.65 ° and 153.37 °, respectively. Our fabricated omniphobic firmer showed superomniphobicity (static contact angle > 150 °) with various low surface tension liquids we tested.

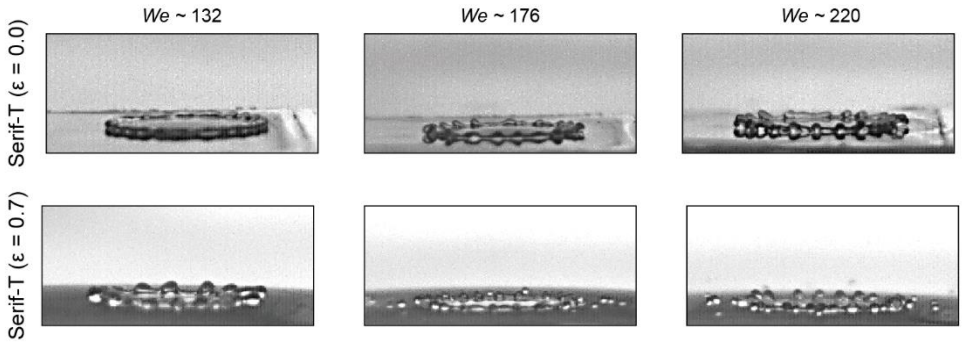

Fig. S8. Fragmentation observation of water droplet with different Weber number (*We*) on hierarchical system with serif-T–shaped nanostructures. (A) Fragmentation regime of water droplet with *We* ~ 132, 176, 220 on flat surface with serif-T-shaped nanostructures. **(B)** Fragmentation regime of water droplet with *We* ~ 132, 176, 220 on highly-wrinkled surface (ε = 0.7) with serif-T-shaped nanostructures.

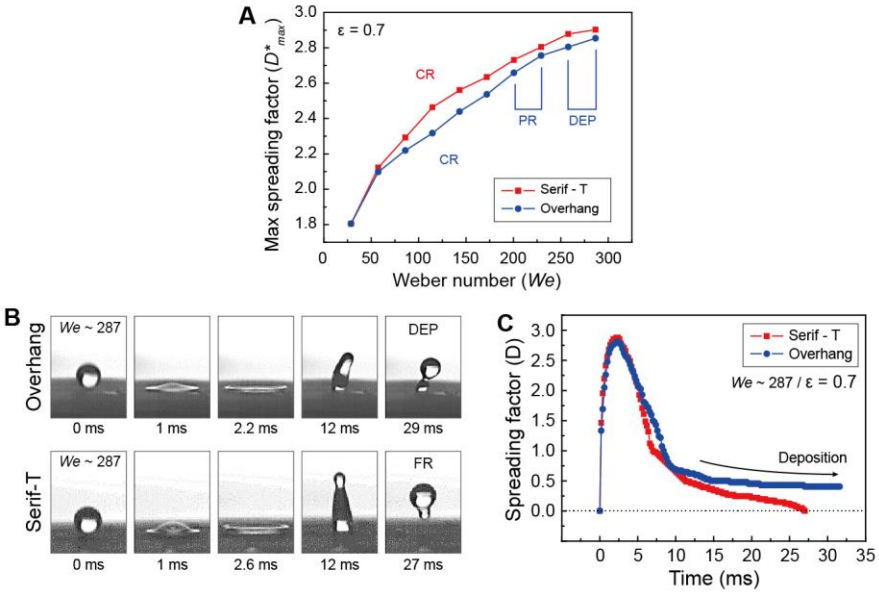

Fig. S9. Bouncing-off behaviors after ethylene glycol droplet impacts on highly wrinkled surface with overhang- and serif-T–shaped nanostructures. (A) bouncing-off phenomena of ethylene glycol droplets with different *We* on hierarchical surface studded with different nanostructures. **(B)** Snapshots showing different bouncing-off behaviors of ethylene glycol (*We* ~ 287) on hierarchical surface with different nanostructures and **(C)** spreading factor from impact to bouncing-off as a function of time.

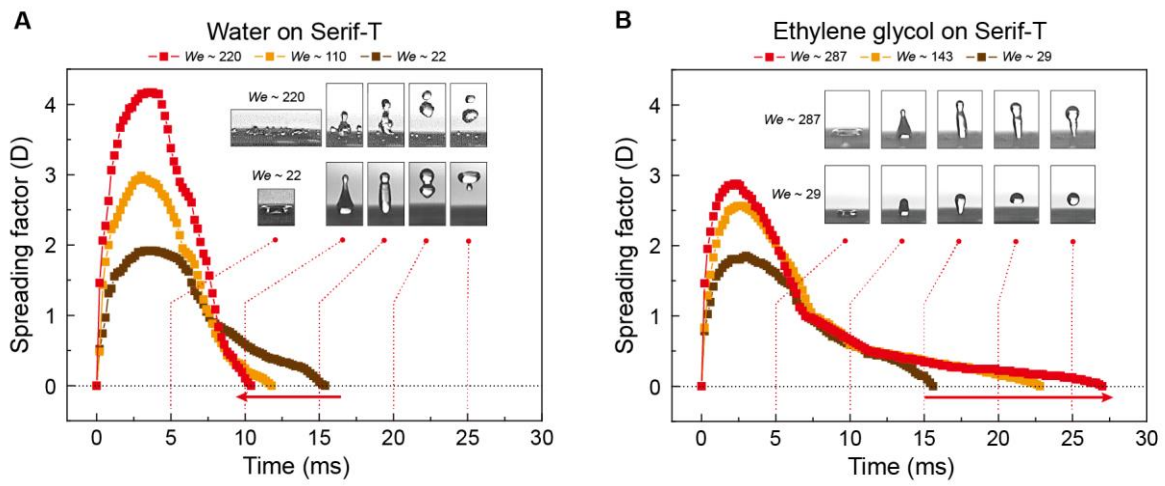

Fig. S10. Contact time analysis of ethylene glycol and water on hierarchical serif-T–shaped nanostructures surface with various *We*. (A) Contact time measurement of water droplets (*We* ~ 22, 110, 220) on highly-wrinkled serif-T surface. Insets are snapshots of the bouncing droplets with different time scale. **(B)** Contact time measurement of ethylene glycol droplets (*We* ~ 29, 143, 287) on highly-wrinkled serif-T surface. Insets are snapshots of the bouncing droplets with different time scale.

Movie Captions

Movie S1. Bouncing behavior of water on the different nanostructures. Water droplets bouncing-off behaviors with *We* ~ 220 on hierarchical system with different kinds of nanostructures (disk-, overhang-, and serif-T-shaped). The highly-wrinkled ($\mathcal{E}$ = 0.7) hierarchical system showed complete rebound (CR) behaviors regardless of nanostructure types. Fragmentation of water droplets was observed due to applied high *We*. This video supports the results in Fig. 4A. Videos were filmed at 5000 fps and were replayed at normal speed.

Movie S2. Contact time comparison of water. Comparison of contact time for water droplets on different morphologies of hierarchical system. The systems are disk-flat, disk-wrinkled, serif-T-flat, and serif-T-wrinkled from left to right. The measured contact times were 23.4, 13.6, 18.8, and 10.4 ms from left to right set. Although all compared system showed complete rebound (CR) behaviors, different affinity with liquids yielded difference of contact time. This video supports the results in Fig. 4E, right. Videos were filmed at 5000 fps and were replayed at normal speed.

Movie S3. Bouncing test of ethylene glycol on the overhang and the serif-T wrinkles. Ethylene glycol droplets bouncing-off behaviors with *We* ~ 287 on hierarchical system studded with overhang- and serif-T shaped nanostructures. In this condition of droplet impact, the ethylene glycol penetrated into overhang hierarchical system resulting in deposition (DEP) behavior. However, the serif-T nanostructures system showed complete rebound (CR) behavior. This video supports the result in Fig. 5A and 5B. Videos were filmed at 5000 fps and were replayed at normal speed.

Movie S4. Bouncing test of ethanol on serif-T samples. Complete rebound (CR) behavior of ethanol droplet with *We* ~ 53 on highly-wrinkled surface with serif-T-shaped nanostructures. Droplet of ethanol was released from syringe at 5 cm height from the sample. This video supports the result in Fig. 5C and 5D. Video was filmed at 5000 fps and were replayed at normal speed.

.